Electrochimica Acta 275 (2018) 208–217

Contents lists available at ScienceDirect

Electrochimica Acta

journal homepage: www.elsevier.com/locate/electacta

Performance of $La_{0.8}Sr_{0.2}Ga_{0.8}Mg_{0.2}O_3$-based SOFCs with atmospheric plasma sprayed La-doped CeO_2 buffer layer

Li-Shuang Wang, Cheng-Xin Li*, Chang-Jiu Li, Guan-Jun Yang

State Key Laboratory for Mechanical Behavior of Materials, School of Materials Science and Engineering, Xi'an Jiaotong University, Xi'an, Shaanxi Province 710049, PR China

ARTICLE INFO

Article history:
Received 26 November 2017
Received in revised form
17 March 2018
Accepted 14 April 2018
Available online 16 April 2018

Keywords:
SOFCs
LDC
Atmospheric plasma spraying
Stability

ABSTRACT

$Ce_{0.6}La_{0.4}O_2$ (LDC) is a promising buffer layer for preventing chemical reactions between a doped-$LaGaO_3$ electrolyte and Ni-based anode in intermediate-temperature solid oxide fuel cells (SOFCs). In the present work, first, the chemical compatibility between $La_{0.8}Sr_{0.2}Ga_{0.8}Mg_{0.2}O_3$ (LSGM) powders and LDC powders is evaluated. Subsequently, an LDC buffer layer is prepared via atmospheric plasma spraying (APS) at different deposition temperatures using powders that have particle sizes larger than 30 μm. The effects of deposition temperature on the microstructure and ionic conductivity are investigated. Cells with an optimized APS LDC interlayer between the NiO containing anode and LSGM electrolyte are tested with humidified H_2 as fuel and ambient air as the oxidation. At 750 °C, the maximum power density of cells with the APS LDC interlayer is 460 mW/cm^2. In addition, a stability test of ~400 h at 650 °C under a constant current density of 250 mW/cm^2 is carried out, and the cell with the optimized APS LDC interlayer is stable. Therefore, APS is a viable alternative approach for fabricating an LDC interlayer for SOFCs using the LSGM electrolyte.

1. Introduction

Solid oxide fuel cells (SOFCs) have been widely investigated as an efficient and environmentally friendly technology for converting chemical energy to electrical energy [1,2]. For efficient commercialization, low-cost alloy materials can be used in SOFCs as interconnectors instead of expensive ceramic materials [3], and the operating temperature of SOFCs can be reduced from high temperature (800–1000 °C) to intermediate temperature (600–800 °C). Reducing the operating temperature is also an effective means of solving the sealing problem [4]. However, the ionic conductivity of a traditional electrolyte material (yttria-stabilized zirconia, YSZ) decreases significantly with a reduced operating temperature. Therefore, it is essential to use alternative electrolytes that have high ionic conductivity at an intermediate temperature. Doped ceria, such as Ga doped ceria (GDC) or Sm doped ceria (SDC), have high ionic conductivity at a lower operating temperature [5]. However, the major drawback of GDC or SDC is the mixed ionic and electronic conduction property because of the reduction of Ce^{4+} to Ce^{3+} that occurs under the fuel reducing atmosphere. Sr and Mg doped lanthanum-gallate ($La_{0.8}Sr_{0.2}Ga_{0.8}Mg_{0.2}O_3$, LSGM) has a perovskite structure and is considered to be a possible electrolyte material at 600–800 °C because of its high ionic conductivity, negligible electronic conductivity, and excellent chemical stability over a wide range of oxygen partial pressures [6,7].

However, when the sintering temperature was higher than 1250 °C, the NiO-containing cermet anode reacted with the LSGM electrolyte. Also, a secondary phase that had high resistance formed at the anode/electrolyte interface, and this resulted in degraded cell performance [8]. Moreover, the reaction of Ni and LSGM resulted in the formation of a La-nickel oxide that has high resistance even at an operating temperature of 600 °C [9]. $Ce_{0.6}La_{0.4}O_2$ (LDC) is considered to be an effective buffer layer for minimizing reaction and interdiffusion between the NiO-containing anode and an LSGM electrolyte [10,11]. The traditional method for preparing an LDC buffer layer and LSGM electrolyte on the anode is usually a conventional wet process followed by cosintering [12,13]. However, the sintering of LDC is rather difficult, and therefore, after cosintering, the sintering density of LDC is much lower than that of LSGM [14,15]. Therefore, it is difficult to form a dense LDC buffer layer using an LSGM electrolyte via the cosintering method. The porous LDC layer may result in the diffusion of Ni from the anode and an

* Corresponding author.
E-mail address: licx@mail.xjtu.edu.cn (C.-X. Li).

https://doi.org/10.1016/j.electacta.2018.04.101
0013-4686/

increase in the total ohmic resistance. Therefore, increasing the LDC density may be beneficial for improving cell performance and long-term stability.

It was reported that, for LSGM-based SOFCs, the reactivity between LSGM and CeO_2-based materials is dominated by a La diffusion mechanism [16–18]. At the interface of LSGM and CeO_2-based materials, the gradient of La results in La diffusion from LSGM into CeO_2-based material, and this causes $LaSrGa_3O_7$ to appear during the cell fabrication process. Therefore, the reaction between GDC or SDC and LSGM is inevitable at high temperature.

Although LDC may prevent La diffusion from LSGM, the chemical compatibility of LDC and LSGM is influenced by the composition of LDC (specifically, the ratio of Ce to La). Andrievskaya et al. reported that the solubility of La_2O_3 in CeO_2 was ~50 mol % [19]. A detailed investigation was reported by Huang and his colleagues regarding the effects of LDC composition on the chemical stability of LDC and LSGM [10]. In their report, when the molar ratio of Ce to La was 1.5 (that is, 40 mol % La in CeO_2; LDC40), La diffusion was effectively prevented after cosintering LSGM and LDC40 at 1350 °C. However, when the Ce/La molar ratio was decreased to 1.0 (LDC50) or increased to 1.86 (LDC35) a reaction between LSGM and LDC occurred, and a resistive phase was detected. Therefore, it can be concluded that LDC with 40 mol% La in CeO_2 are effective interlayer materials for LSGM-based SOFCs.

Atmospheric plasma spraying (APS) is considered to be a promising processing method for producing SOFC components because of its high efficiency, flexibility, and low cost [20,21]. Previously, APS has been used to deposit porous electrode layers [22,23], dense electrolyte layers [24,25], and protective ceramic layers for metal interconnects [26]. Zhang et al. prepared an scandia-stabilized zirconia electrolyte layer using APS at a deposition temperature of 600 °C and achieved a maximum power density of ~1 W/cm^2 at an operating temperature of 1000 °C [27]. Therefore, it may be possible to prepare a dense buffer layer for SOFCs using APS without high temperature sintering.

However, to the best of our knowledge, an LDC buffer layer prepared using APS for LSGM-based SOFCs has not yet been reported in detail. The purpose of this study is to fabricate an LDC buffer layer for SOFCs via APS using spray powders that have a Ce/La molar ratio of 1.5. First, the chemical compatibility of LDC powders with LSGM and NiO powders was characterized. Second, the effects of deposition temperature on the microstructure and ionic conductivity of LDC deposits were studied. Finally, the output performance and the stability of LSGM-supported cells with an optimized APS LDC coating were investigated.

2. Experimental section

2.1. Materials

A commercially available spray-dried spherical LDC powders (Tianyao Inc., Qingdao, China) with particle size of 32–45 μm was used to deposit an LDC coating. This powder was provided with a 50% excess of Ce; specifically, the atomic Ce/La ratio was 1.5. As reported in our previous work [28], Ce preferentially evaporates during the APS process, and the spray powder size is important for the Ce loss. When the spray powder size of LDC is > 30 μm, the Ce loss in the APS LDC coatings can be neglected, and the Ce/La ratio is similar to that of the starting powders. Therefore, spray powders with particle sizes larger than 30 μm were used. Typical morphologies of the powders are shown in Fig. 1. The powders had spherical morphologies (Fig. 1a) and were composed of nano- and submicrometer particles, as seen in the magnified images (Fig. 1b).

LSGM was used as an electrolyte to construct electrolyte-supported SOFCs. Commercially available LSGM starting powders (Fuelcellmaterials Inc., USA) were used in this study. The starting powders were uniaxially pressed into a pellet (15 mm diameter, 500 μm thick) by applying a press of 150 MPa and then sintered at

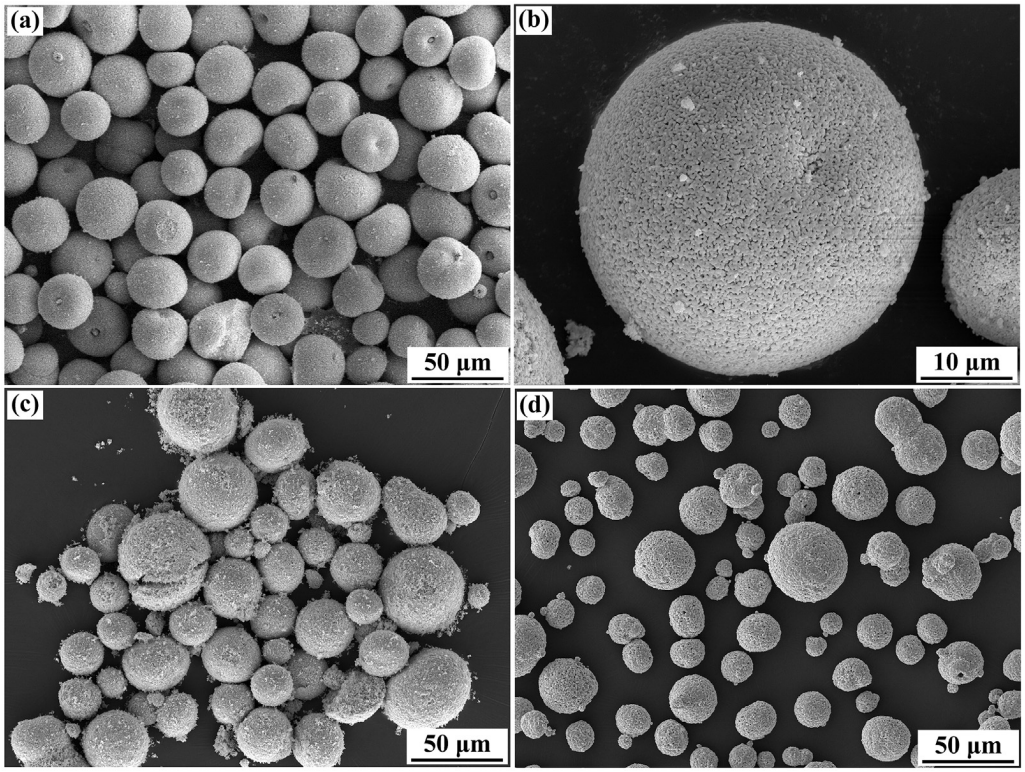

Fig. 1. Morphology of the starting powders: (a) LDC at low magnification, (b) LDC at high magnification, and (c) NiO-GDC and (d) LSCF at low magnification.

1400 °C for 10 h. After sintering, the pellets were ground and polished to obtain electrolyte pellets with a diameter of 13 mm and a thickness of ~350 μm. In addition, commercially available $La_{0.6}Sr_{0.4}Co_{0.2}Fe_{0.8}O_3$ (LSCF) and NiO-GDC spherical powders were used as the cathode material and anode material, respectively. The LSCF powders had a particle size of 5–20 μm (Fig. 1c), and the NiO/GDC powders had a particle size of 30–70 μm (Fig. 1d).

2.2. Study of chemical compatibility

The LDC powders were mixed with NiO and LSGM, respectively, to investigate the chemical compatibility of LDC with NiO and LSGM. Each mixture was in a mass ratio of 1:1 and then heated at 1400 °C for 10 h. X-ray powder diffraction (XRD, Xpert PRO, PANalytical, Netherlands) was used for careful analysis of the phase structures of the mixtures.

2.3. Cell fabrication

Before cell fabrication, sand blasting was used on the LSGM surface to enhance interfacial bonding between the coating and substrate. APS (GP-80, Jiujiang, China) was used to deposit the LDC interlayer on the LSGM support substrate using a plasma arc of 36 KW. The deposition parameters were similar to those used in the previous report [28]. The flow rates of Ar and H_2 were set to 60 slpm and 6 slpm, respectively. The spray distance was 80 mm. Results from our previous study revealed that the critical deposition temperature of LDC was 400 °C [29]. In this study, the LDC interlayer was deposited at a deposition temperature of 500 °C to enhance lamellar interface bonding. To confirm the substrate temperature, the back of the LSGM substrate was preheated using a copper heating stage, and the surface temperature was monitored using an infrared pyrometer (RayRPM30L3U, Raytak, America).

The NiO/GDC anode was then deposited on top of the optimized LDC interlayer using APS with a plasma arc of 36 KW. The coating thickness was controlled to 30–40 μm. A similar APS procedure was also used to deposit an LSCF cathode layer on the other side of the LSGM electrolyte support with a low plasma arc of 30 KW. The effective electrode area of the cell was 0.8 cm^2. The APS deposition parameters are shown in Table 1.

Scanning electron microscopy (SEM, TESCAN, Czech) equipped with an energy dispersing X-ray (EDX) system was used to characterize the microstructures of the LDC coatings and the cells, and XRD was used to analyze the phases of the sintered LSGM. The ionic conductivity of the APS LDC deposits was measured using an AC method described elsewhere [30,31]. First, the free standing LDC deposits were obtained by removing the substrate, and then a silver slurry was pasted onto both sides of the LDC samples in an active area that had a diameter of 8 mm. The paste samples were dried at 180 °C for 30 min and then heated to 800 °C; the samples were then held at 800 °C for 30 min. Electrochemical impedance spectroscopy (EIS, Solartron SI 1260/1287 impedance analyzer) was used to measure the ionic conductivity over a temperature range of 500–800 °C with an applied AC voltage of 25 mV during the cooling stage.

Table 1
Typical APS LDC deposition parameters.

Parameter	Unit	LDC	NiO/GDC	LSCF
Plasma arc power	kW	36	36	30
Plasma arc voltage	V	50	60	50
Plasma arc current	A	720	600	600
Flow rate of Ar	slpm	60	45	60
Flow rate of H_2	slpm	6	4.5	1.5
Spray distance	mm	80	100	100
Deposition temperature	°C	500	<150	<150

2.4. Cell performance test

For electrochemical testing of the cell, silver paste was attached as current collectors and was used on both the cathode and anode sides. The performance of a single cell was tested in a furnace at a heating and cooling rate of 3 °C/min. After reducing the anode at 750 °C for 2 h, the output performance of the cell was measured in a temperature range of 600–750 °C during the cooling stage. The moistened H_2 fuel and air were used at flow rates of 0.1 slpm and 0.15 slpm, respectively. EIS was used with an applied AC voltage of 25 mV to determine the electrochemical properties of the cells. The frequency during the test procedure was in the range of 10^{-1} to 10^5 Hz.

3. Results and discussion

3.1. Reactivity of LDC with LSGM and NiO

It is expected that interfacial reactions deteriorate the output performance of SOFCs because the reaction products that have high resistance increase the ohmic resistance of SOFCs. XRD patterns of the starting LSGM and LDC mixtures and of these mixtures after annealing at 1400 °C for 10 h are shown in Fig. 2. The XRD results showed that the phase structure of the annealed powder mixture was similar to that of the starting powder mixture, and there was no secondary phase detected. This indicates that there was no chemical reactivity between LDC and LSGM. XRD was also used to identify the phase structure of the NiO and LDC mixture after annealing at 1400 °C for 10 h and to analyze the starting powders. The results are shown in Fig. 3. As seen in Fig. 3, the phase structure of the annealed powder mixture was also similar to that of the starting powder mixture (NiO+LDC), and no reaction products were found after the heat treatment. These results are consistent with those previously reported. Huang et al. [10] noted that the reaction of LDC with LSGM and NiO can be avoided when the La content in CeO_2 is 40 mol%, and in this study, the LDC powders that had 40 mol % La content were chemically-stable with LSGM and NiO.

3.2. Microstructure of atmospheric plasma sprayed LDC interlayer

The fractured cross-sectional morphology and the XRD pattern

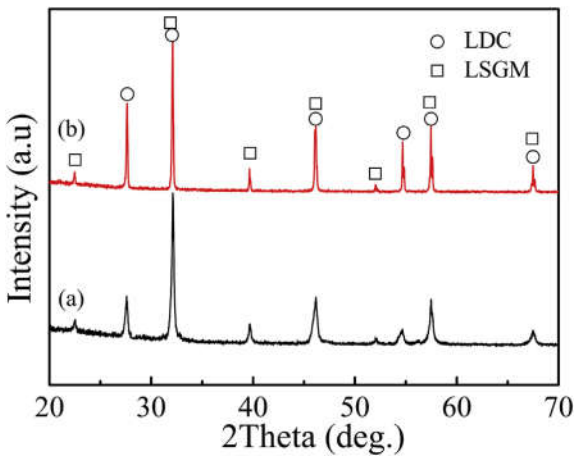

Fig. 2. XRD patterns of a mixture of LSGM and LDC in a 1:1 wt ratio: (a) starting powder mixture and (b) mixture after annealing at 1400 °C for 10 h.

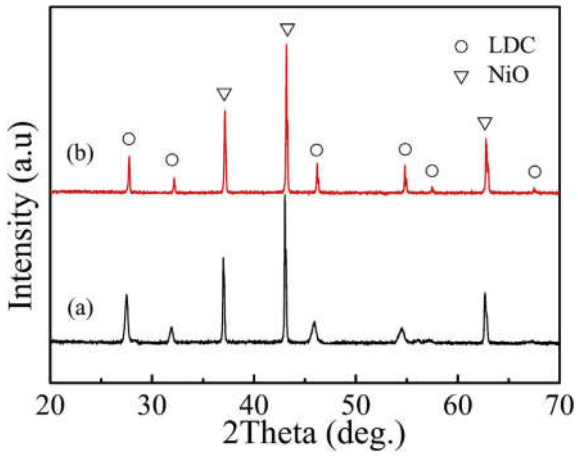

Fig. 3. XRD patterns of a mixture of NiO and LDC in a 1:1 wt ratio: (a) starting powder mixture and (b) mixture after annealing at 1400 °C for 10 h.

of the sintered LSGM pellet are shown in Fig. 4. LSGM has a dense structure with few closed pores after annealing at 1400 °C, and on the basis of the image analysis, the porosity was ~2%. As seen in Fig. 4b, bulk LSGM had a pure perovskite phase, and no secondary phase was detected. Thus, bulk LSGM was suitable for our experiments to use as an electrolyte in SOFCs.

The LDC coatings were deposited at 100 °C, 300 °C, and 500 °C to study the effects of deposition temperature on the microstructure. The ratio of Ce to La in the LDC coatings was confirmed via EDS analysis, and the results are summarized in Table 2. The molar ratios of Ce to La in the LDC deposits were similar to that in the original powder mixture. Thus, in the present study, the Ce/La ratio in the LDC coatings remained the same as that of the original powders and thereby the composition of LDC coatings meets the requirement for using as an buffer layer.

Fractured cross-sectional morphologies of the LDC coatings deposited at different temperature are shown in Fig. 5. When the deposition temperature was 100 °C, the coating had a lamellar structure with a nonbonded interface (indicated by arrow "A" in Fig. 5a) and vertical cracks (indicated by arrow "B" in Fig. 5a). When the deposition temperature was increased to 300 °C, a columnar grain with a length of 5–6 μm was observed in single splats, and there were a few interlamellar cracks. When the deposition temperature was further increased to 500 °C, the columnar crystals grew continuously through several lamellas and the crystals had a length of ~10 μm. Moreover, it is difficult to identify the unbonded interface between lamellas in the cross-section. Simultaneously,

Table 2
Chemical compositions of LDC powders and deposits.

Sample	Ce/La, molar ratio
LDC powders	1.507 ± 0.012
LDC deposits (100 °C)	1.495 ± 0.009
LDC deposits (300 °C)	1.503 ± 0.005
LDC deposits (500 °C)	1.490 ± 0.011

the amount of vertical cracks decreased because the quenching stress of the splats was significantly decreased via the substrate preheating during plasma spraying [27]. As a result, the APS LDC coating became denser with an increase in the deposition temperature. As previously reported, the lamellar bonding ratio for conventionally thermal sprayed ceramic coatings is lower than ~33% [32,33]. With an increase in the deposition temperature, the bonding ratio improved. Xing et al. reported that when the deposition temperature was increased from room temperature to 686 °C, the interlamellar bonding ratio of the plasma sprayed YSZ coating increased from 32% to 50% [30]. SEM observations in the present study suggest that the splats are well bonded and that the APS LDC coating became dense when the deposition temperature was 500 °C (Fig. 5c).

3.3. Ionic conductivity of APS LDC coatings deposited at different temperatures

Free-standing LDC deposits were obtained for electrical characterization after the substrate was removed. The total ionic conductivity of LDC as a function of test temperature is shown in Fig. 6. The ionic conductivity of the LDC deposit increased with an increase in temperature (Fig. 6a), and this suggests that the dependence of the LDC electrical properties with respect to temperature is similar to that of other solid ion conductors, such as YSZ, GDC, and LSGM. For the LDC deposits, the conductivity increased with an increased in deposition temperature. At 800 °C, the LDC coatings that were deposited at 500 °C showed conductivity values of 0.015 S/cm, which is the highest of the LDC deposits examined in this study. This value was more than twice that of the LDC deposited at 100 °C (~0.0067 S/cm), and it was 75% of the bullk conductivity (0.020 S/cm at 800 °C). The ionic conductivity values of bulk LDC are from the literature, as reported by Hong et al. [34]. It has been reported that deflects in the electrolyte decrease ionic conductivity because the ionic conductivity is directly proportional to the O^{2-} transport number [35,36]. A significant number of previous studies have examined the influence of microstructure on the conductance of oxide-ion conductors, and most of these works

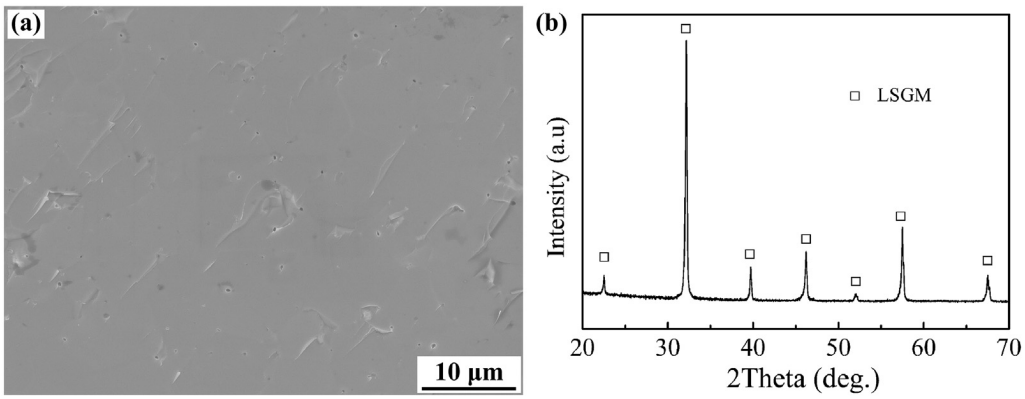

Fig. 4. (a) SEM images of the fractured cross-sectional morphology and (b) phase structure of an LSGM pellet after sintering at 1400 °C for 10 h.

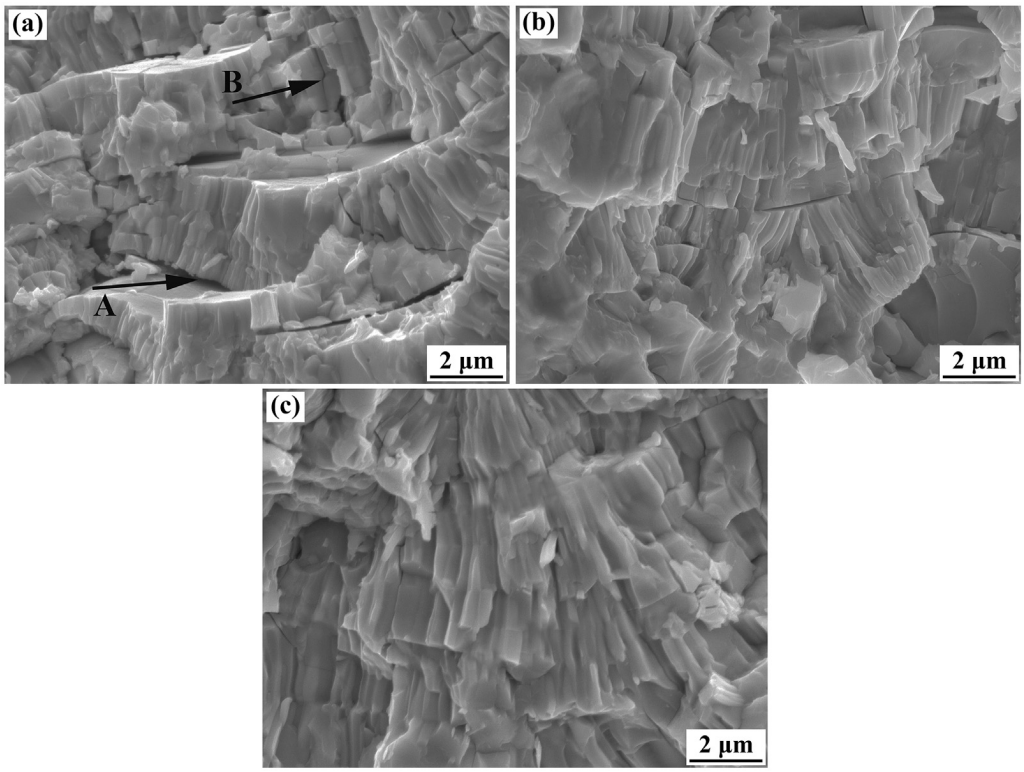

Fig. 5. SEM images of fractured cross sectional morphologies of LDC coatings deposited at different temperatures: (a) 100 °C, (b) 300 °C, and (c) 500 °C.

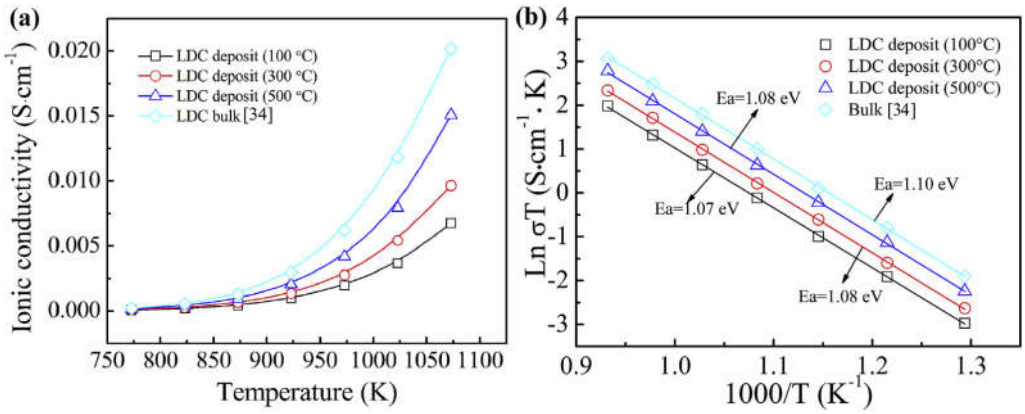

Fig. 6. (a) Total ionic conductivity of the LDC samples and (b) Arrhenius plots of the total ionic conductivity of LDC samples.

have focused on sintered samples, such as YSZ [37,38] and GDC [39]. It has been reported that the total ionic conductance decreases with an increase in porosity because of the detrimental effects of pores on ionic transport. For APS coatings, ionic conductivity in the parallel direction is nearly twice as high as that in the perpendicular direction because of the different microstructures [40]. According to Xing et al., the limited interfacial bonding of the lamellar structure reduces the ionic conductivity of stabilized zirconia deposits to one-fifth of that of the bulk material [30]. The nonbonded interface between lamellas hampers O^{2-} migration and results in a decrease in the ionic conductivity. Thus, it is reasonable that the ionic conductivity of the LDC deposit decreases with a decrease in deposition temperature, and this is mainly attributed to the different lamellar bonding ratios.

The Arrhenius plots of the electrical conductivities of the LDC deposits are shown in Fig. 6b. The activation energies (Ea) were estimated from the slopes of the corresponding Arrhenius plots. The Ea values of the LDC deposits obtained at 100 °C, 300 °C, and 500 °C were ~1.07 eV, 1.08 eV, and 1.08 eV, respectively. These values are similar to the Ea values of bulk LDC (~1.10 eV) [34], and this indicates that the ion migration modes of the APS LDC coatings are consistent with bulk LDC.

3.4. Cell performance

According to the literature [41–43], an interlayer with a high density is preferable, mainly for two reasons. First, the LDC interlayer prevents the diffusion of La and Ni from the LSGM electrolyte and anode, respectively. This requires sufficient necking, such as a dense microstructure, between grains. Second, high ionic

conductivity of the interlayer decreases the ohmic resistance. Therefore, on the basis of the microstructure and the ionic conductivity values of the APS LDC coatings reported in Sections 3.2 and 3.3, the LSGM-based cells were assembled using an APS LDC interlayer deposited at a temperature of 500 °C. The polished cross-sectional microstructure of the half-cell is shown in Fig. 7. As seen in Fig. 7a, the thickness of the LDC interlayer was 10–20 μm and that of the NiO/GDC anode was 30–40 μm. The LDC interlayer was well bonded with the LSGM electrolyte layer and with NiO-GDC anode layer. Additionally, the large surface roughness of the APS LDC coating provided many third phase boundaries (TPBs) for anode reactions. As shown in Fig. 7b, the thickness of the LSCF cathode was 20–30 μm. The LSCF cathode was adhered well to the LSGM electrolyte layer, and the porous structure simultaneously contributed to oxygen transfer. Moreover, the semi-molten LSCF particles provided more TPBs for cathode reactions.

The output performance of the cell is shown in Fig. 8. The open circuit voltage (OCV) was ~1.1 V (Fig. 8a), and this is very close to the theoretical value. This result indicates that, in this study, the cell sealing met the requirement. At an operating temperature of 600 °C, the maximum power density (MPD) was ~112 mW/cm^2. When the operating temperature was increased to 650 °C, 700 °C, and 750 °C, the MPD increased to ~198 mW/cm^2, 307 mW/cm^2, and 460 mW/cm^2, respectively. In a previous report, a single cell with a 500 μm-thick LSGM, SDC interlayer, SDC+NiO anode, and $La_{0.8}Sr_{0.2}CoO_{3-\delta}$ (LSCo) cathode obtained an MPD of 370 mW/cm^2 at 750 °C [10]. The thickness of LSGM was 350 μm in this study, and the cell performance was comparable to that of the reported cell with an SDC interlayer. Although the LDC has a relatively lower conductivity than the SDC at a given temperature, the cell performance with an APS LDC interlayer in this study is acceptable.

Fig. 8b shows a typical impedance spectrum of a single cell measured under open circuit conditions at 600–750 °C. The ohmic resistance (R_o), polarization resistance (R_p), and total resistance (R_t) can be determined from Fig. 8b. The intercept at high frequency of the spectrum represents the ohmic resistance, the intercept at low frequency of the spectrum represents the total cell resistance, and the widths of the impedance arcs provide the values of the polarization resistance. The resistance values (R_o, R_p, and R_t) determined from Fig. 8b are listed in Table 3. The ohmic resistance was 0.53 Ω cm^2 at 750 °C. The values for the conductivity of bulk LSGM and the LDC deposits at 750 °C were 0.07 S/cm and 0.0085 S/cm, respectively, and therefore the calculated ohmic resistance of LSGM and LDC was 0.65 Ω cm^2, which is slightly larger than the measured value (0.53 Ω cm^2 at 750 °C). Bi et al. also obtained lower specific resistance for LDC-LSGM compared to the calculated values [44]. The lower measured ohmic resistance may be attributed to Co diffusion from the cathode to LSGM [45]. Additionally, Singman et al. reported that the ionic conductivity of LDC improves with low oxygen pressure [14]. The lower specific resistance indicates that the APS LDC interlayer is effective for preventing interactions between LSGM and the NiO-based anode, and therefore high resistance phases did not form. Also, the low ohmic resistances demonstrated that the mixed conductivity of APS LDC contributed to oxide ion transport from the electrolyte to the anode.

The ohmic resistances were higher than the polarization resistances at a specific operating temperature, and this was because of the thicker electrolyte thickness. The values of polarization resistance for the cells were similar to the values reported by Hwang and his colleagues [46], and in their report, both of the electrodes were also deposited using APS. It is, thus, estimated that well-bonded electrode/electrolyte interfaces (Fig. 7) were achieved in this study.

Fig. 9 shows a schematic diagram of the electrochemical reaction on the anode side with an APS LDC interlayer. First, addition of an LDC interlayer succeeds in suppressing interfacial chemical reactions between the Ni-based anode and the LSGM electrolyte. Second, the APS LDC interlayer deposited at 500 °C consisted of elongated columnar grains that had a dense microstructure and decreased ohmic resistance. Furthermore, the reducing atmosphere on the anode side created a mixed Ce^{4+} and Ce^{3+} valence in the LDC layer; this helped to catalyze the dissociative chemisorption of the fuel [34,47]. Also, the reduction of Ce^{4+} increased the oxygen-vacancy concentration of LDC, and this increased the O^{2-} transport across the buffer layer, which increased TPBs on the anode side [47]. Therefore, an APS LDC interlayer with low resistance prevented dangerous interfacial chemical reactions and also promoted fuel cell reactions.

3.5. Stability of the cell

A stability test of the cell was carried out under a constant current density of 250 mA cm^{-2} at 650 °C. The cell was tested for ~400 h, and the cell voltage and power density as functions of time are shown in Fig. 10. The cell voltage and power density appears to remain constant with time. After the stability test, the LSGM/LDC/Ni-GDC interface microstructure was observed using SEM and the attached EDX line-scan technique. Fig. 11 shows the SEM image in back scattering electron (BSE) mode and EDX line scan graphs of Ni and La across AB on the cross section of the LSGM/LDC/Ni-GDC after stability test for 400 h. These coatings are well bonded and no large crack is observed in both interfaces of LSGM/LDC and LDC/Ni-GDC. Clearly, the diffusion of Ni and La did not occur and no distinct reaction layer was detected in the LDC/LSGM interface. The stable

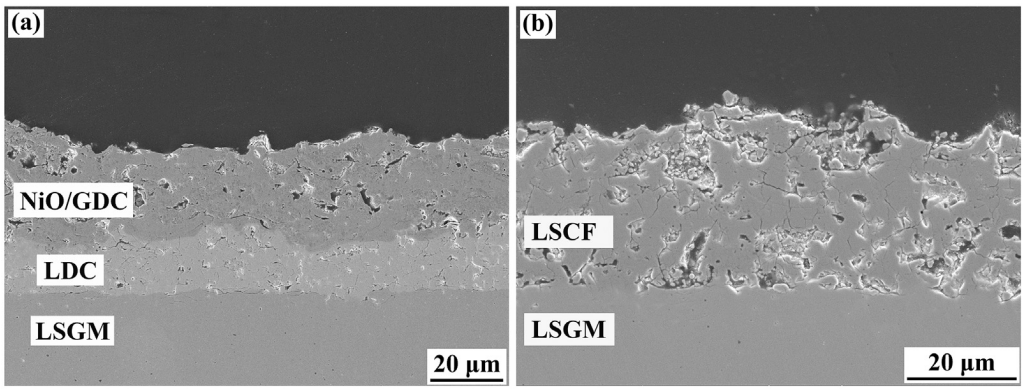

Fig. 7. Polished cross-sectional microstructure of an LSGM-based SOFCs: (a) anode side and (b) cathode side.

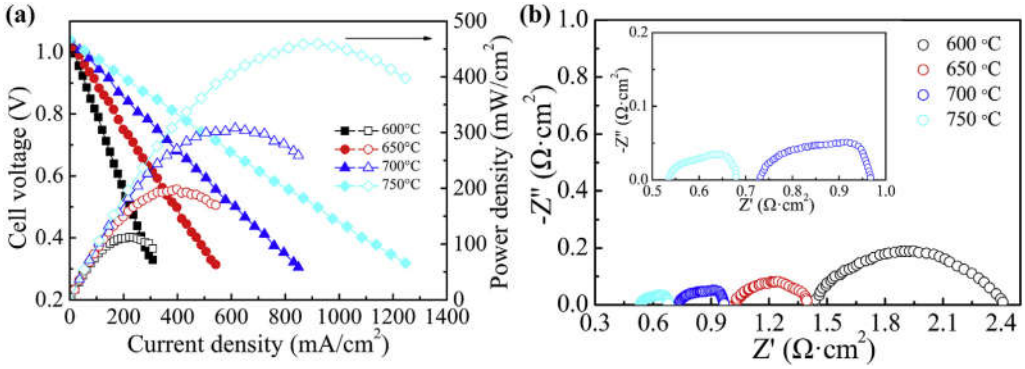

Fig. 8. Electrochemical properties at various temperatures for LSGM-based cells with an LDC interlayer: (a) cell voltage (solid symbols) and power density (open symbols) as a function of current density and (b) impedance spectrum of a single cell.

Table 3
Resistance values at different operation temperatures of a single cell with an APS LDC interlayer.

Operating temperature (°C)	R_o (Ω·cm^2)	R_p (Ω·cm^2)	R_t (Ω·cm^2)
600	1.4	1.0	2.4
650	1.0	0.4	1.4
700	0.73	0.24	0.97
750	0.53	0.15	0.68

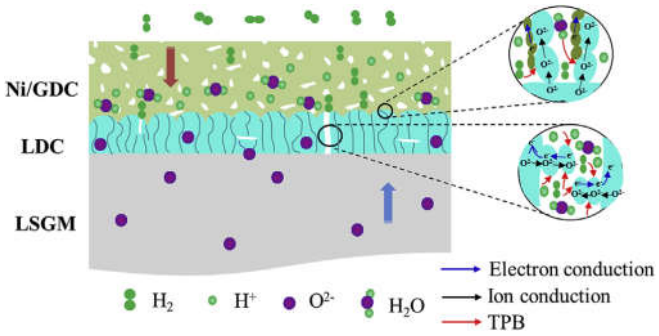

Fig. 9. Schematic diagram of electrochemical reactions on the anode side.

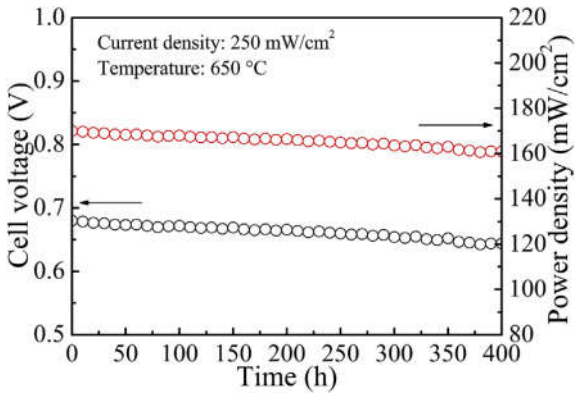

Fig. 10. Cell voltage (black) and power density (red) as a function of time at 650 °C under a constant current density of 250 mA cm^{-2}. (For interpretation of the references to colour in this figure legend, the reader is referred to the Web version of this article.)

cell performance and the EDX results suggests that the interfacial chemical reactions on the anode side can be neglected, which was consistent with the result reported by Huang et al. [10]. In their report, no secondary phases were found when the La_2O_3 doping level was lower than 50 mol %. The APS LDC interlayer successfully prevented Ni or La diffusion. In addition, the stable cell voltage indicates that the resistance of the cell remained constant over time. Therefore, it can be concluded that interfacial interactions did not occur during the long term stability test at 650 °C.

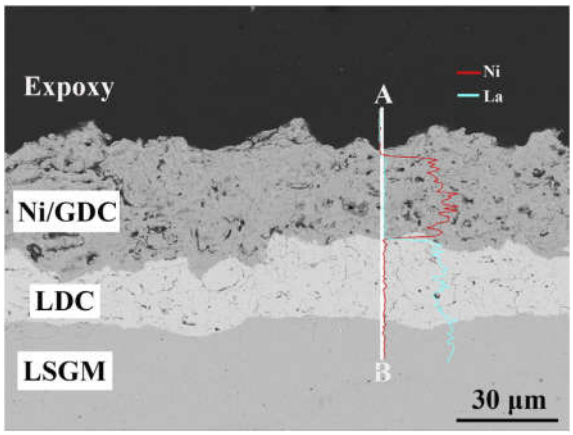

Fig. 11. BSE image and the corresponding EDS line map across AB on the cross-section of LSGM/LDC/Ni-GDC after stability test at 650 °C for 400 h.

For Ni-based SOFCs, it is essential to observe the microstructure change in the anode material. Because the grain growth would lead to reduced TPBs, thereby resulting in the degradation of cell performance [48]. Fig. 12 showed the microstructure of Ni-based cermet anode and the corresponding EDX mapping of Ni before and after cell stability test for 400 h at 650 °C. During the spraying, NiO/GDC particles melted and impacted on the substrate. Thus, each splat contained both NiO and GDC. Because the amount of GDC. vol% in the starting powders was 70%, and therefore GDC was acted as skeleton. Pores in the plasma spray coatings consisted of nonbonded lamellar interfaces, intra-lamellar vertical cracks and three-dimensional voids [49]. After the reduction, the pores were further broadened due to the volume shrinkage. Fuel gas and oxidation gas can easily pass through these interconnected pores, and thus thermal sprayed coating can be employed as porous electrodes in SOFCs. After operating for 400 h, as shown in Fig. 12b and d, the microstructure of Ni/GDC coating was similar with the original coatings (Fig. 12a and c). The unchanged microstructure may be attributed to two reasons. On one hand, the enhanced connection of NiO and GDC in the anode was achieved by APS, because the agglomerated NiO/GDC powders were used as feedstock. Therefore, the skeleton of GDC in the anode effectively

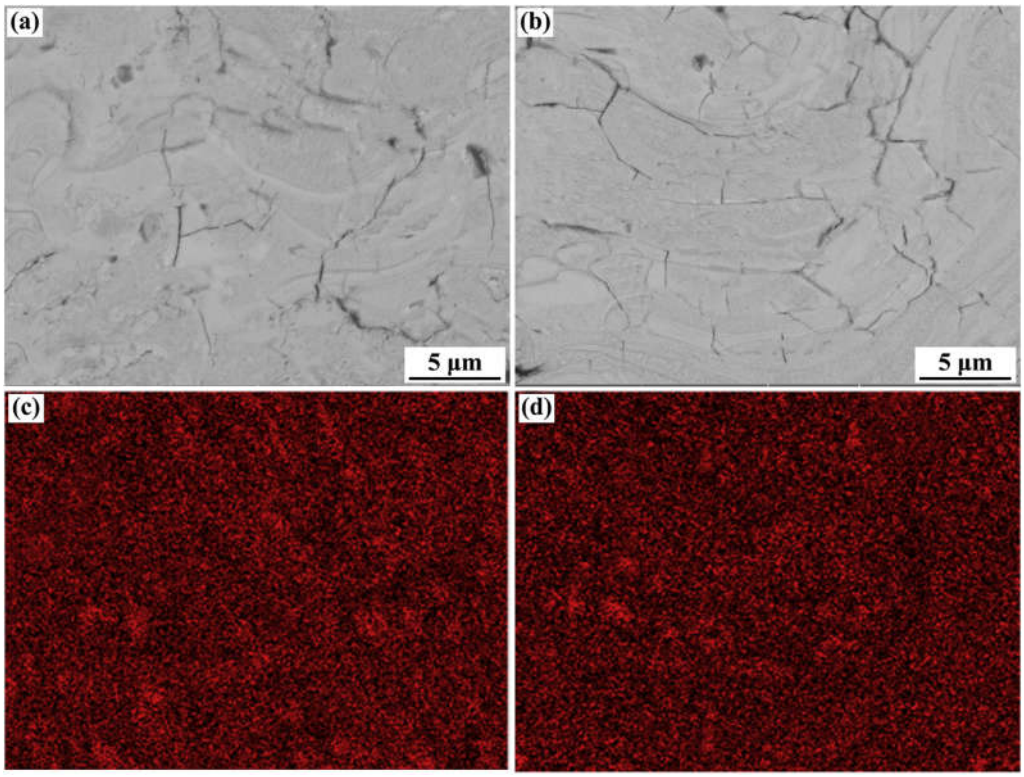

Fig. 12. Microstructure (a) and the corresponding Ni map (c) of Ni/GDC anode before stability test, microstructure (b) and the corresponding Ni map (d) after stability test for 400 h.

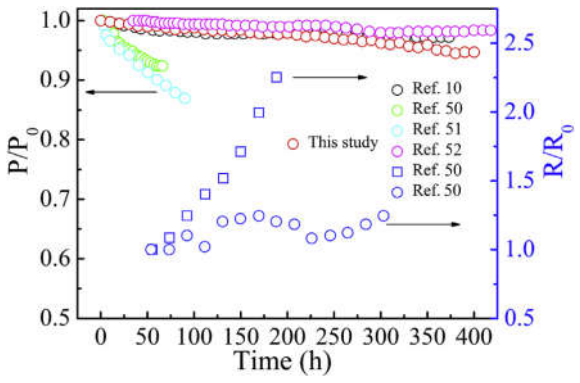

Fig. 13. P/P_0 and R/R_0 ratios vs. time for the present SOFC and for SOFCs previously reported in Refs [10,50–52]. (without LDC interlayer (square), with LDC interlayer (circle)).

prevent the coarsening of Ni during the cell operation. On the other hand, the lower operating temperature significantly decreased the grain growth. Therefore, the changing of anode microstructure can be neglected.

A comparison of the performance stability of SOFCs that had an LSGM electrolyte fabricated via cofiring with the performance stability results obtained in this study are presented in Fig. 13. The power density at the initial time and that at a specific time are denoted as P_0 and P, respectively. Similarly, the polarization resistance at the initial time and that at a specific time are denoted as R_0 and R, respectively. The ratios of P/P_0 and R/R_0 were used to characterize the cell stability performance. The compositions of these cells are shown in Table 4. The performance of SOFCs with LDC interlayers appear to be stable [10,50–52], and the performance of SOFCs without an LDC interlayer deteriorated because of increasing polarization resistance [50]. The slight decrease in the power density of the cell was induced by coarsening of Ni, and this was confirmed by Guo and his coauthors [51]. As a result, adding an LDC interlayer is effective for maintaining the stability of cells with an LSGM electrolyte.

4. Conclusions

A LDC interlayer in an SOFC was prepared via atmospheric plasma spraying and was inserted between the LSGM electrolyte layer and the Ni-based anode layer to prevent interfacial reactions. LDC was proven to be chemically stable with LSGM and NiO at high temperature. The microstructure and ionic conductivity of the APS

Table 4
Compositions of LSGM electrolyte SOFCs.

Cell sources	Anode	Anode buffer layer	Electrolyte		Cathode
Present work	Ni-GDC	LDC (10–20 μm)	LSGM (350 μm)		LSCF
Ref. [10]	Ni-LDC	LDC	LSGM (600 μm)		$SrCo_{0.8}Fe_{0.2}O_{3-\delta}$
Ref. [50]	Ni-LDC	LDC (15 μm)	LSGM (1 mm)		LSCF-LSGM
Ref. [51]	Ni-SDC	LDC (12 μm)		LSGM (11 μm)	LSCF-LSGM
Ref. [52]	Ni-LDC	LDC (30 μm)		LSGM	$SrCo_{0.8}Fe_{0.2}O_{3-\delta}$

LDC coatings are influenced by deposition temperature. Specifically, the coating became dense with an increase in the deposition temperature. At a deposition temperature of 500 °C, the LDC coating was composed of long columnar crystals and showed good interlamellar bonding. Also, the ionic conductivity of the LDC coatings increased with an increase in deposition temperature. When the deposition temperature was 500 °C, the ionic conductivity of the LDC coating was 0.015 S/cm at 800 °C, and this value was nearly 75% of that for bulk LDC. The performance of the LSGM-based SOFC with an optimized APS LDC interlayer, APS anode, and APS cathode was evaluated at an intermediate temperature. At 750 °C, the cell with an LSGM electrolyte thickness of 350 μm showed ohmic resistance of 0.53 Ω cm^2 and an MPD of 460 mW/cm^2. The cell showed a constant output performance for 400 h at 650 °C, and this suggests that the APS LDC interlayer suppressed interfacial reactions. Therefore, thermal spray is a low cost and effective method for preparing an LDC interlayer for LSGM-based SOFCs.

Acknowledgements

The work was supported by National Key R&D Program of China (Grant No.2017YFB0306100).

References

[1] B.C.H. Steele, A. Heinzel, Materials for fuel-cell technologies, Nature 414 (6861) (2001) 345–352.
[2] O. Yamamoto, Solid oxide fuel cells: fundamental aspects and prospects, Electrochim. Acta 45 (15–16) (2000) 2423–2435.
[3] E. Ivers-Tiffee, A. Weber, D. Herbstritt, Materials and technologies for SOFC-components, J. Eur. Ceram. Soc. 21 (10–11) (2001) 1805–1811.
[4] S. Ghosh, A. Das Sharma, P. Kundu, R.N. Basu, Glass-ceramic sealants for planar IT-SOFC: a bilayered approach for joining electrolyte and metallic interconnect, J. Electrochem. Soc. 155 (5) (2008) B473–B478.
[5] H. Inaba, H. Tagawa, Ceria-based solid electrolytes-Review, Solid State Ionics 83 (1–2) (1996) 1–16.
[6] T. Ishihara, H. Matsuda, Y. Takita, Doped $LaGaO_3$ perovskite-type oxide as a new oxide ionic conductor, J. Am. Chem. Soc. 116 (9) (1994) 3801–3803.
[7] E. Djurado, M. Labeau, Second phases in doped lanthanum gallate perovskites, J. Eur. Ceram. Soc. 18 (10) (1998) 1397–1404.
[8] J.H. Joo, D.Y. Kim, G.M. Choi, Effects of anode firing temperature on the performance of the lanthanum-gallate thick-film-supported SOFC, Solid State Ionics 192 (1) (2011) 523–526.
[9] S.L. Zhang, C.X. Li, C.J. Li, Chemical compatibility and properties of suspension plasma-sprayed $SrTiO_3$-based anodes for intermediate-temperature solid oxide fuel cells, J. Power Sources 264 (2014) 195–205.
[10] K.Q. Huang, J.H. Wan, J.B. Goodenough, Increasing power density of LSGM-based solid oxide fuel cells using new anode materials, J. Electrochem. Soc. 148 (7) (2001) A788–A794.
[11] M. Feng, J.B. Goodenough, K.Q. Huang, C. Milliken, Fuel cells with doped lanthanum gallate electrolyte, J. Power Sources 63 (1) (1996) 47–51.
[12] Y.B. Lin, S.A. Barnett, Co-firing of anode-supported SOFCs with thin $La_{0.9}Sr_{0.1}Ga_{0.8}Mg_{0.2}O_{3-\delta}$ electrolytes, Electrochem. Solid St. 9 (6) (2006) A285–A288.
[13] D. Lee, J.H. Han, E.G. Kim, R.H. Song, D.R. Shin, Performance of strontium- and magnesium-doped lanthanum gallate electrolyte with lanthanum-doped ceria as a buffer layer for IT-SOFCs, J. Power Sources 185 (1) (2008) 207–211.
[14] D. Singman, Preliminary evaluation of ceria-lanthana as a solid electrolyte for fuel cells, J. Electrochem. Soc. 113 (5) (1966) 1410–1416.
[15] H. Yoshida, H. Deguchi, K. Miura, M. Horiuchi, T. Inagaki, Investigation of the relationship between the ionic conductivity and the local structures of singly and doubly doped ceria compounds using EXAFS measurement, Solid State Ionics 140 (3–4) (2001) 191–199.
[16] M. Hrovat, A. Ahmad-Khanlou, Z. Samardzija, J. Holc, Interactions between lanthanum gallate based solid electrolyte and ceria, Mater. Res. Bull. 34 (12–13) (1999) 2027–2034.
[17] M. Hrovat, J. Holc, S. Bernik, D. Makovec, Subsolidus phase equilibria in the NiO-CeO_2 and La_2O_3-CeO_2-Fe_2O_3 systems, Mater. Res. Bull. 33 (8) (1998) 1175–1183.
[18] M. Hrovat, Z. Samardzija, J. Holc, S. Bernik, Subsolidus phase equilibria in the La_2O_3-Ga_2O_3-CeO_2 system, J. Mater. Res. 14 (12) (1999) 4460–4462.
[19] E.R. Andrievskaya, O.A. Kornienko, A.V. Sameljuk, A. Sayir, Phase relation studies in the CeO_2-La_2O_3 system at 1100-1500 °C, J. Eur. Ceram. Soc. 31 (7) (2011) 1277–1283.
[20] R. Hui, Z.W. Wang, O. Kesler, L. Rose, J. Jankovic, S. Yick, R. Maric, D. Ghosh, Thermal plasma spraying for SOFCs: applications, potential advantages, and challenges, J. Power Sources 170 (2) (2007) 308–323.
[21] D. Stover, D. Hathiramani, R. Vassen, R.J. Damani, Plasma-sprayed components for SOFC applications, Surf. Coating. Tech. 201 (5) (2006) 2002–2005.
[22] C.X. Li, C.J. Li, L.J. Guo, Effect of composition of NiO/YSZ anode on the polarization characteristics of SOFC fabricated by atmospheric plasma spraying, Int. J. Hydrogen Energy. 35 (7) (2010) 2964–2969.
[23] E.S.C. Fan, J. Kuhn, O. Kesler, Suspension plasma spraying of $La_{0.6}Sr_{0.4}Co_{0.2}Fe_{0.8}O_{3-\delta}$ cathodes: influence of carbon black pore former on performance and degradation, J. Power Sources 316 (2016) 72–84.
[24] C.J. Li, C.X. Li, Y.Z. Xing, M. Gao, G.J. Yang, Influence of YSZ electrolyte thickness on the characteristics of plasma-sprayed cermet supported tubular SOFC, Solid State Ionics 177 (19–25) (2006) 2065–2069.
[25] J. Oberste Berghaus, J.G. Legoux, C. Moreau, R. Hui, C. Deces-Petit, W. Qu, S. Yick, Z. Wang, R. Maric, D. Ghosh, Suspension HVOF spraying of reduced temperature solid oxide fuel cell electrolytes, J. Therm. Spray Technol. 17 (5–6) (2008) 700–707.
[26] J. Puranen, M. Pihlatie, J. Lagerbom, G. Boleili, J. Laakso, L. Hyvarinen, M. Kylmalahti, O. Himanen, J. Kiviaho, L. Lusvarghi, P. Vuoristo, Post-mortem evaluation of oxidized atmospheric plasma sprayed Mn-Co-Fe oxide spinel coatings on SOFC interconnectors, Int. J. Hydrogen Energy. 39 (30) (2014) 17284–17294.
[27] S.L. Zhang, C.X. Li, C.J. Li, G.J. Yang, Z.H. Han, Scandia-stabilized zirconia electrolyte with improved interlamellar bonding by high-velocity plasma spraying for high performance solid oxide fuel cells, J. Power Sources 232 (2013) 123–131.
[28] L.S. Wang, S.L. Zhang, T. Liu, C.J. Li, C.X. Li, G.J. Yang, Dominant effect of particle size on the CeO_2 preferential evaporation during plasma spraying of $La_2Ce_2O_7$, J. Eur. Ceram. Soc. 37 (4) (2017) 1577–1585.
[29] S.W. Yao, C.J. Li, J.J. Tian, G.J. Yang, C.X. Li, Conditions and mechanisms for the bonding of a molten ceramic droplet to a substrate after high-speed impact, Acta Mater. 119 (2016) 9–25.
[30] Y.Z. Xing, C.J. Li, C.X. Li, G.J. Yang, Influence of through-lamella grain growth on ionic conductivity of plasma-sprayed yttria-stabilized zirconia as an electrolyte in solid oxide fuel cells, J. Power Sources 176 (1) (2008) 31–38.
[31] G.R. Li, G.J. Yang, C.X. Li, C.J. Li, Strain-induced multiscale structural changes in lamellar thermal barrier coatings, Ceram. Int. 43 (2) (2017) 2252–2266.
[32] C.J. Li, A. Ohmori, The lamellar structure of a detonation gun sprayed Al_2O_3 coating, Surf. Coating. Tech. 82 (3) (1996) 254–258.
[33] C.J. Li, G.J. Yang, C.X. Li, Development of particle interface bonding in thermal spray coatings: a review, J. Therm. Spray Technol. 22 (2–3) (2013) 192–206.
[34] J.E. Hong, T. Inagaki, S. Ida, T. Ishihara, Improved sintering and electrical properties of La-doped CeO_2 buffer layer for intermediate temperature solid oxide fuel cells using doped $LaGaO_3$ film prepared by screen printing process, J. Solid State Electrochem. 16 (4) (2012) 1493–1502.
[35] E. Iguchi, S. Nakamura, F. Munakata, M. Kurumada, Y. Fujie, Ionic conduction due to oxygen diffusion in $La_{0.8}Sr_{0.2}GaO_{3-\delta}$ electrolyte, J. Appl. Phys. 93 (6) (2003) 3662–3664.
[36] S.K. Tadokoro, T.C. Porfirio, R. Muccillo, E.N.S. Muccillo, Synthesis, sintering and impedance spectroscopy of 8 mol% yttria-doped ceria solid electrolyte, J. Power Sources 130 (1–2) (2004) 15–21.
[37] M.C. Steil, F. Thevenot, M. Kleitz, Densification of yttria-stabilized zirconia-Impedance spectroscopy analysis, J. Electrochem. Soc. 144 (1) (1997) 390–398.
[38] I.R. Gibson, G.P. Dransfield, J.T.S. Irvine, Sinterability of commercial 8 mol% yttria-stabilized zirconia powders and the effect of sintered density on the ionic conductivity, J. Mater. Sci. 33 (17) (1998) 4297–4305.
[39] D. Perez-Coll, E. Sanchez-Lopez, G.C. Mather, Influence of porosity on the bulk and grain-boundary electrical properties of Gd-doped ceria, Solid State Ionics 181 (21–22) (2010) 1033–1042.
[40] C. Zhang, C.J. Li, G. Zhang, X.J. Ning, C.X. Li, H.L. Liao, C. Coddet, Ionic conductivity and its temperature dependence of atmospheric plasma-sprayed yttria stabilized zirconia electrolyte, Mat. Sci. Eng. B-Solid. 137 (1–3) (2007) 24–30.
[41] X.D. Zhu, K.N. Sun, S.R. Le, N.Q. Zhang, Q. Fu, X.B. Chen, Y.X. Yuan, Improved electrochemical performance of NiO-$La_{0.45}Ce_{0.55}O_{2-\delta}$ composite anodes for IT-SOFC through the introduction of a $La_{0.45}Ce_{0.55}O_{2-\delta}$ interlayer, Electrochim. Acta 54 (2) (2008) 862–867.
[42] D.W. Jung, C. Kwak, S. Seo, K.S. Moon, I.T. Han, J.S. Kim, Role of the gadolinia-doped ceria interlayer in high-performance intermediate-temperature solid oxide fuel cells, J. Power Sources 361 (2017) 153–159.
[43] A. Mai, V.A.C. Haanappel, F. Tietz, D. Stover, Ferrite-based perovskites as cathode materials for anode-supported solid oxide fuel cells-Part II. Influence of the CGO interlayer, Solid State Ionics 177 (19–25) (2006) 2103–2107.
[44] Z.H. Bi, B.L. Yi, Z.W. Wang, Y.L. Dong, H.J. Wu, Y.C. She, M.J. Cheng, A high-performance anode-supported SOFC with LDC-LSGM bilayer electrolytes, Electrochem. Solid St. 7 (5) (2004) A105–A107.
[45] T. Horita, K. Yamaji, N. Sakai, H. Yokokawa, A. Weber, E. Ivers-Tiffee, Stability at $La_{0.6}Sr_{0.4}CoO_{3-\delta}$ cathode/$La_{0.8}Sr_{0.2}Ga_{0.8}Mg_{0.2}O_{2.8}$ electrolyte interface under current flow for solid oxide fuel cells, Solid State Ionics 133 (3–4) (2000) 143–152.
[46] C.S. Hwang, T.J. Hwang, C.H. Tsai, C.L. Chang, S.F. Yang, M.H. Wu, C.Y. Fu, Effect of plasma spraying power on LSGM electrolyte of metal-supported solid oxide fuel cells, Ceram. Int. 43 (2017) S591–S597.
[47] K.Q. Huang, J.B. Goodenough, A solid oxide fuel cell based on Sr- and Mg-doped $LaGaO_3$ electrolyte: the role of a rare-earth oxide buffer, J. Alloys.

Compd. 303 (2000) 454–464.
[48] D. Simwonis, F. Tietz, D. Stover, Nickel coarsening in annealed Ni/8YSZ anode substrates for solid oxide fuel cells, Solid State Ionics 132 (3–4) (2000) 241–251.
[49] C.J. Li, A. Ohmori, Relationships between the microstructure and properties of thermally sprayed deposits, J. Therm. Spray Technol. 11 (3) (2002) 365–374.
[50] W.Q. Gong, S. Gopalan, U.B. Pal, Performance of intermediate temperature (600-800 ^{o}C) solid oxide fuel cell based on Sr and Mg doped lanthanum-gallate electrolyte, J. Power Sources 160 (1) (2006) 305–315.
[51] W.M. Guo, J. Liu, Y.H. Zhang, Electrical and stability performance of anode-supported solid oxide fuel cells with strontium- and magnesium-doped lanthanum gallate thin electrolyte, Electrochim. Acta 53 (13) (2008) 4420–4427.
[52] J.H. Wan, J.Q. Yan, J.B. Goodenough, LSGM-based solid oxide fuel cell with 1.4 W/cm^2 power density and 30 day long-term stability, J. Electrochem. Soc. 152 (8) (2005) A1511–A1515.